Dnmt3a deficiency in the skin causes focal, canonical DNA hypomethylation and a cellular proliferation phenotype

David Y. Chen[a], Ian M. Ferguson[a], Krista A. Braun[a,b], Leslie A. Sutton[a], Nichole M. Helton[b], Sai Mukund Ramakrishnan[b], Amanda M. Smith[b], Christopher A. Miller[b], and Timothy J. Ley[b,1]

[a]Division of Dermatology, Department of Medicine, Washington University School of Medicine, Saint Louis, MO 63110; and [b]Section of Stem Cell Biology, Division of Oncology, Department of Medicine, Washington University School of Medicine, Saint Louis, MO 63110

Contributed by Timothy J. Ley, February 27, 2021 (sent for review November 4, 2020; reviewed by Stephen B. Baylin and Gordon D. Ginder)

DNA hypomethylation is a feature of epidermal cells from aged and sun-exposed skin, but the mechanisms responsible for this methylation loss are not known. Dnmt3a is the dominant de novo DNA methyltransferase in the skin; while epidermal Dnmt3a deficiency creates a premalignant state in which keratinocytes are more easily transformed by topical mutagens, the conditions responsible for this increased susceptibility to transformation are not well understood. Using whole genome bisulfite sequencing, we identified a focal, canonical DNA hypomethylation phenotype in the epidermal cells of Dnmt3a-deficient mice. Single-cell transcriptomic analysis revealed an increased proportion of cells with a proliferative gene expression signature, while other populations in the skin were relatively unchanged. Although total DNMT3A deficiency has not been described in human disease states, rare patients with an overgrowth syndrome associated with behavioral abnormalities and an increased risk of cancer often have heterozygous, germline mutations in *DNMT3A* that reduce its function (Tatton-Brown Rahman syndrome [TBRS]). We evaluated the DNA methylation phenotype of the skin from a TBRS patient with a germline *DNMT3A*^{R882H} mutation, which encodes a dominant-negative protein that reduces its methyltransferase function by ∼80%. We detected a focal, canonical hypomethylation phenotype that revealed considerable overlap with hypomethylated regions found in Dnmt3a-deficient mouse skin. Together, these data suggest that DNMT3A loss creates a premalignant epigenetic state associated with a hyperproliferative phenotype in the skin and further suggest that DNMT3A acts as a tumor suppressor in the skin.

DNMT3A | DNA methylation | epigenetic | epidermis | premalignant

Aging and sun exposure are the most important epidemiologic risk factors for the development of skin cancer in populations with lightly pigmented skin. Although there are no registries to accurately account for the incidence of nonmelanoma skin cancers, treatment utilization for keratinocyte carcinomas sharply increases with advancing age (1). The accumulation of genetic mutations from UV light exposure clearly contributes to age-dependent increases in skin cancer; however, sun-damaged skin can harbor a remarkable number of driver mutations while remaining clinically normal (2). This suggests that nonmutational factors may also influence skin cancer susceptibility. The contribution of epigenetic perturbations (including alterations in DNA methylation) to cancer susceptibility is incompletely understood (3, 4). Aged, sun-exposed epidermal skin cells in older people develop DNA methylation changes, compared to the sun-protected skin of younger individuals (5). It is not yet clear whether altered activity of DNA methyltransferases or demethylases, cellular population shifts, or changes in cellular signaling or other modifying factors are responsible for this change.

DNA methyltransferases are responsible for CpG methylation and comprise two functional groups: 1) the maintenance methyltransferase DNMT1, which copies methylation marks to the CpGs of newly synthesized DNA; and 2) the de novo methyltransferases DNMT3A and DNMT3B, which are responsible for modifying unmethylated cytidine residues in a CpG dinucleotide context as well as some aspects of maintenance methylation (6, 7). DNA methylation is important for normal skin development and function. Mice with *Dnmt1* deficiency in skin develop progressive alopecia, resulting in >50% hair loss over a year, while *DNMT1* knockdown in human keratinocytes causes premature differentiation (8, 9). Similarly, the knockdown of either *DNMT3A* or *DNMT3B* reduces the clonogenic potential of cultured human keratinocytes (10). Importantly, Dnmt3a (but not Dnmt3b) has tumor suppressor activity in the classic 7,12-dimethylbenz[a]anthracene (DMBA)/12-*O*-tetradecanoylphorbol-13-acetate (TPA) chemical carcinogenesis model, with shortened latency and a higher tumor burden in Dnmt3a-deficient skin (11); however, the precise epigenetic changes that contribute to the premalignant, susceptible state have not yet been clearly defined.

In humans, there is considerable evidence that alterations in DNA methylation machinery may play a role in skin cancer pathogenesis. Both precancerous actinic keratoses (AKs) and squamous cell carcinomas (SCCs) exhibit hypomethylation of CpGs in lamina-associated domains, hypermethylation of CpG islands, and increased *DNMT3B* expression (12). *DNMT3A* is expressed at lower levels in AKs and SCCs, compared to healthy skin (11). Finally, somatic *DNMT3A* mutations have been identified in 11% (33/304) of patients from three studies of basal cell carcinoma (BCC) and SCC (cbioportal.org); *DNMT3B* was mutated in 8% (12/146) of

Significance

Keratinocyte carcinomas are the most common malignancies in fair-skinned patients. Increased age and sun exposure are important skin cancer risk factors and have been associated with a loss of DNA methylation in the human epidermis. Complete Dnmt3a deficiency in mouse skin creates a premalignant state, but the mechanisms responsible for this phenomenon are not clear. This study demonstrates that Dnmt3a deficiency in murine epidermis causes focal, canonical DNA hypomethylation and an increased proportion of cells with a proliferative gene expression signature. Understanding the mechanisms responsible for the premalignant state may be important for defining novel preventative or therapeutic strategies for skin cancers.

Author contributions: D.Y.C. and T.J.L. designed research; D.Y.C., I.M.F., K.A.B., L.A.S., N.M.H., and T.J.L. performed research; D.Y.C., I.M.F., L.A.S., S.M.R., A.M.S., C.A.M., and T.J.L. analyzed data; and D.Y.C. and T.J.L. wrote the paper.

Reviewers: S.B.B., Johns Hopkins University School of Medicine; and G.D.G., Virginia Commonwealth University.

The authors declare no competing interest.

[1]To whom correspondence may be addressed. Email: timley@wustl.edu.

This article contains supporting information online at https://www.pnas.org/lookup/suppl/doi:10.1073/pnas.2022760118/-/DCSupplemental.

Published April 12, 2021.

cases and *DNMT1* in 15% (45/304) (13–15). Many of the mutations in *DNMT3A* in these tumors were localized to the methyltransferase domain, or were predicted to cause protein truncations that would be expected to disrupt its function and potentially cause haploinsufficiency.

Dnmt3a deficiency in murine bone marrow cells results in a focal, canonical DNA hypomethylation phenotype (16–18) that is associated with the development of hematopoietic malignancies (17, 19, 20). DNA hypomethylation in Dnmt3a-deficient marrow is reversible with DNMT3A reexpression, and remethylation occurs in an orderly fashion with predictable kinetics and high fidelity (18). Germline mutations in *DNMT3A* are strongly associated with an overgrowth syndrome (Tatton-Brown-Rahman syndrome [TBRS]) that is associated with a potentially increased risk of acute myeloid leukemia (AML) (21, 22). Finally, acquired mutations of *DNMT3A* in older individuals are the most common cause of hematopoietic clonal expansion, which is associated with an increased risk of AML development (23–26). Indeed, *DNMT3A* mutations are among the most common initiating mutations in adults with de novo AML; mutations at amino acid position R882 (most frequently R882H) represent the most common mutational hot spot in this gene (27).

In this study, we evaluate the premalignant epigenetic phenotype of Dnmt3a-deficient skin and identify changes that could potentially contribute to its role in increasing susceptibility to transformation. We then relate these findings to the skin methylation phenotype of a TBRS patient with a germline $DNMT3A^{R882H}$ mutation.

Results

***Dnmt3a* Deficiency in Epidermal Keratinocytes Results in a Focal, Canonical DNA Hypomethylation Phenotype.** Mice with homozygous *Dnmt3a* deficiency develop normally but die within 3 wk of birth (28). To study the effects of Dnmt3a deficiency in the skin, we therefore used transgenic mice expressing *Cre* recombinase under the control of the Keratin 14 (*Krt14*) promoter, which exhibits a well-established pattern of expression that affects the epidermal skin and its appendages (29). With appropriate crosses, we obtained mice that were wild type (WT) for *Dnmt3a* (*Krt14-Cre*$^-$ × $Dnmt3a^{flox/flox}$, hereafter "$Dnmt3a^{WT}$"), heterozygous (*Krt14-Cre*$^+$ × $Dnmt3a^{flox/+}$, hereafter "$Dnmt3a^{HET}$"), or homozygous for the floxed allele (*Krt14-Cre*$^+$ × $Dnmt3a^{flox/flox}$, hereafter "$Dnmt3a^{KO}$"). The floxing efficiency of the $Dnmt3a^{flox/flox}$ alleles in epidermal cells with *Krt14*-Cre was >90%, resulting in a complete loss of Dnmt3a protein expression (*SI Appendix*, Fig. S1*A*).

Whole genome bisulfite sequencing (WGBS) was used to assess DNA methylation of isolated murine epidermal cells. $Dnmt3a^{KO}$ mice exhibited a small but significant decrease in global DNA methylation in all annotated regions examined, including CpG islands, island shores, island shelves, gene bodies, promoters, enhancers, and transcriptional start sites (Fig. 1 *A*, *Top*). Loss of one allele of Dnmt3a ($Dnmt3a^{HET}$) resulted in a statistically significant change in methylation from the $Dnmt3a^{WT}$ in all regions except gene bodies. On a global scale, the overall decrease in CpG methylation was very small, similar to what has been observed in hematopoietic tissues (Fig. 1 *B*, *Top*) (18, 30).

We identified differentially methylated regions (DMRs) between $Dnmt3a^{WT}$ and $Dnmt3a^{KO}$ samples using previously described approaches (18, 30). DMRs were defined as having greater than 10 CpGs with a mean methylation difference of more than 0.2 (i.e., 20%) between $Dnmt3a^{WT}$ and $Dnmt3a^{KO}$ skin, with a false discovery rate (FDR) of less than 0.05. Adjacent DMRs within 50 base pairs were merged. Based on these criteria, we identified 23,983 DMRs with an average size of 0.95 kilobases (Kb), encompassing 23.53 megabases (Mb) of DNA, which represents 0.87% of the genome (Dataset S1). Virtually all DMRs were hypomethylated (23,981/23,983; 99.99%), and the degree of hypomethylation did not vary based on their location in annotated genomic regions (Fig. 1 *A*, *Bottom*). Skin from $Dnmt3a^{HET}$ mice demonstrated a more subtle methylation phenotype at these DMRs (Fig. 1 *B*, *Bottom*). The DMRs in Dnmt3a-deficient skin are represented by a heatmap, where each column represents an independent mouse, and each row, the mean methylation value of an individual DMR for all samples (Fig. 1*C*). There is remarkable consistency (i.e., canonicality) among the methylation phenotypes at each DMR among independent mice with the same genotypes. The methylation values of the $Dnmt3a^{HET}$ samples are plotted passively and exhibit an intermediate level of methylation at many DMRs (Fig. 1*C*), demonstrating that haploinsufficiency for Dnmt3a also has a methylation phenotype in the skin (Fig. 1 *A* and *B*).

Dnmt3a-dependent DMRs occur most commonly within gene bodies; 16.4% of all annotated protein-coding genes were found to have at least one DMR. DNA methylation within most CpG islands is low in $Dnmt3a^{WT}$ skin, as expected. A small fraction of these islands (142/16,923; 0.89%) exhibit significantly higher methylation than total CpG islands in $Dnmt3a^{WT}$ skin, and these rare islands generally become hypomethylated in $Dnmt3a^{KO}$ skin (Fig. 1 *D* and *A*, *Bottom*). These DMRs usually represent intragenic CpG islands, of which ∼65% are methylated in human embryonic stem cells (31). Indeed, 129/142 (91%) $Dnmt3a^{KO}$ DMRs associated with CpG islands are located within gene bodies. The shores and shelves flanking CpG islands exhibited greater proportions of DMRs (3.7% and 8.85%, respectively), while the methylation of transcriptional start sites (TSSs) was minimally affected by Dnmt3a deficiency (0.86%, Fig. 1*D*). The methylation pattern near the *G0s2* gene is shown as an example of a $Dnmt3a^{KO}$ DMR that occurs in a gene body (Fig. 1*E*). This gene was found to be up-regulated in $Dnmt3a^{KO}$ skin tumors (11).

Dnmt3a Deficiency Results in a Distinct Transcriptional Phenotype. Dnmt3a deficiency does not result in any gross abnormalities in unperturbed skin (11). Further, flow cytometric evaluation of cellular populations within the skin revealed minimal differences between $Dnmt3a^{WT}$ and $Dnmt3a^{KO}$ (*SI Appendix*, Fig. S1*B*). To interrogate the transcriptomic consequences of Dnmt3a deficiency, we employed single-cell RNA sequencing to analyze adult murine epidermis in telogen (the resting phase of the hair cycle). We analyzed two mice from each genotype ($Dnmt3a^{WT}$ and $Dnmt3a^{KO}$) at 9 to 10 wk of age; 10,482 cells from $Dnmt3a^{WT}$ and 15,403 cells from $Dnmt3a^{KO}$ met quality standards. Unbiased clustering based on expression signatures defined subpopulations of cells in the skin (Fig. 2*A*) that were remarkably similar among all four samples (Fig. 2*B*).

Unique populations segregated into distinct clusters with graph-based clustering and are represented by uniform manifold approximation and projection (UMAP) dimension reduction plots shown in Fig. 2*A* (32). In total, 19 clusters were identified by unbiased methods (Louvain method graph-based clustering, Dataset S3), which were subsequently categorized into 10 populations based on well-established, experimentally validated markers representing known populations in the epidermis (Fig. 2 *A*, *Right*). The hair follicle bulge (HFB) contains follicular stem cells and is marked by *Cd34* expression (33), while the upper hair follicle (uHF) is marked by beta defensin (*Defb6*) expression (34, 35). Subdivided into the isthmus and infundibulum, the upper hair follicle bridges the follicle with the interfollicular epidermis and sebaceous gland, which is marked by the expression of *Mgst1* (34). The basal interfollicular epithelium (bIFE) contains slow cycling, proliferative cells that act as an epidermal stem cell compartment (36), and is marked by "basal" keratin gene expression (*Krt5* and *Krt14*), as well as *Thbs1* (37). The suprabasal interfollicular epithelium (sbIFE) is postmitotic and marked by the expression of the genes that encode keratins *Krt1* and *Krt10* and an early differentiation marker metallothionein *Mt4* (34). Melanocytes were marked by expression of the genes encoding tyrosinase (*Tyr*) and dopachrome tautomerase (*Dct*). Inflammatory cells, including T cells and Cd207-expressing Langerhans cells, comprised 1.3% and 1.1% of total cells in the samples, respectively. Finally, one population

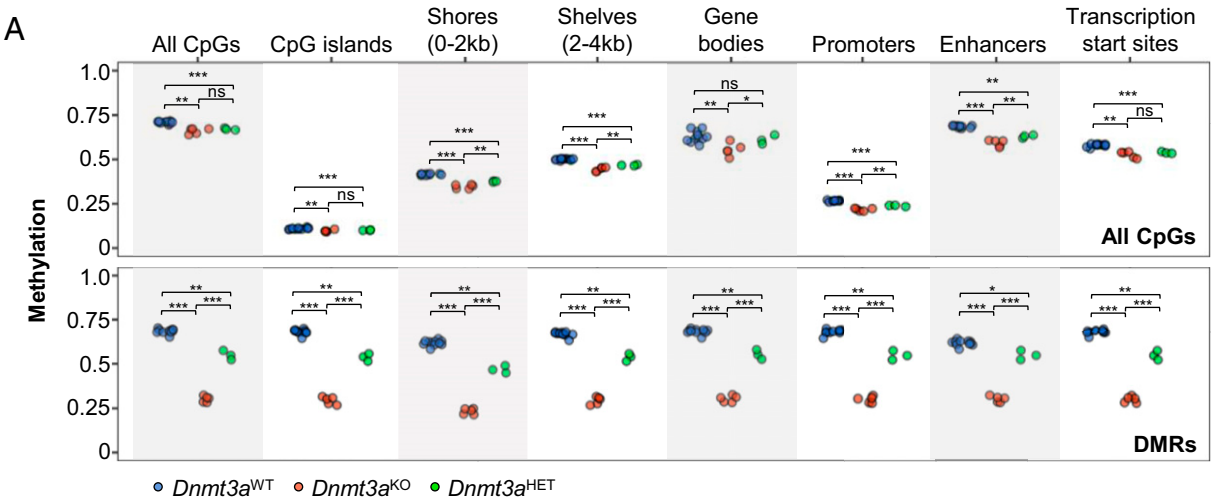

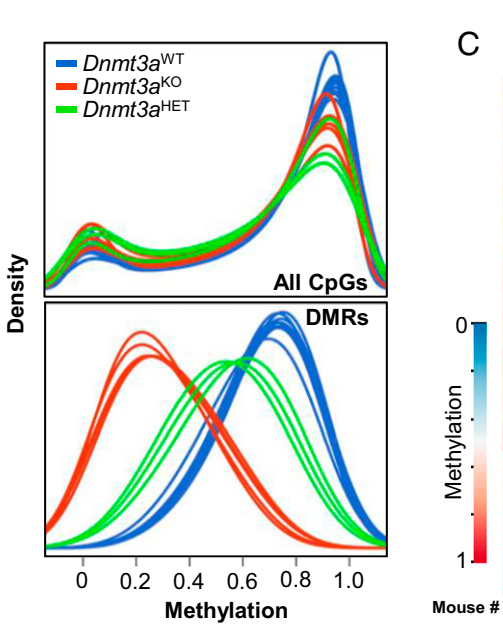

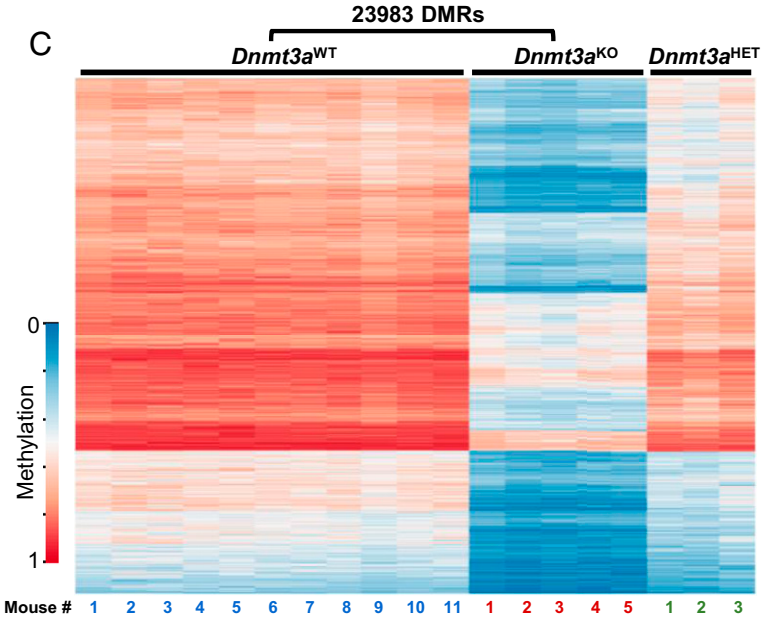

D

	Total	DMR	% Total
CpG island	16023	142	0.89
Shore	43441	1608	3.70
Shelf	30221	2676	8.85
Gene body	22026	3612*	16.40
Promoter	68260	1084	1.59
Enhancer	22271	705	3.17
TSS	20564	177	0.86

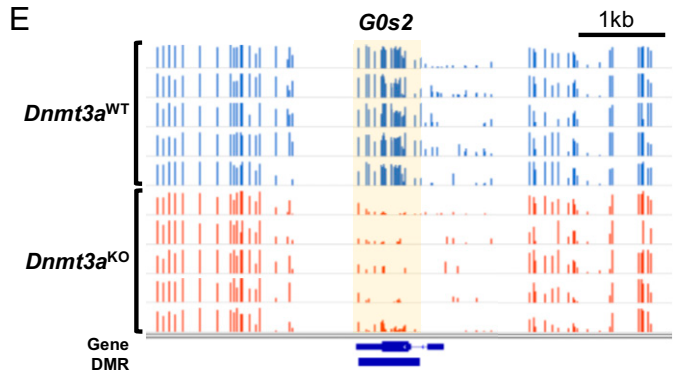

Fig. 1. Dnmt3a deficiency results in focal, canonical CpG methylation loss in murine epidermal cells. (*A*) WGBS of isolated murine epidermal cells, comparing independent samples from 11 *Dnmt3a*^{WT} vs. 5 *Dnmt3a*^{KO} vs. 3 *Dnmt3a*^{HET} mice. Dot plots represent average methylation values over annotated regions for all CpGs (*Top*) and for DMRs within each annotated region (*Bottom*). Significance was determined by Student's *t* test with denotation of "ns" for not significant and levels of significance as * adjusted $P < 0.05$, ** $P < 0.01$, *** $P < 0.001$. (*B*) Methylation density plots for the indicated genotypes across all genomic CpGs (*Top*) and at DMRs (*Bottom*). (*C*) Targeted deficiency of Dnmt3a (*Krt14*-Cre^{+} × *Dnmt3a*$^{fl/fl}$, *Dnmt3a*^{KO}) results in 23,983 DMRs in epidermal cells compared to wild-type control, *Dnmt3a*^{WT}. Heatmap representation of WGBS data demonstrates DMRs defined by differences between *Dnmt3a*^{WT} vs. *Dnmt3a*^{KO} epidermal cells. Heterozygosity for Dnmt3a (*Krt14*-Cre^{+} × *Dnmt3a*$^{fl/+}$, *Dnmt3a*^{HET}) results in an intermediate phenotype. Each column represents an independent mouse. (*D*) Annotated regions associated with DMRs. *Of 16,315 DMRs involving gene bodies, 3,612 unique genes are involved. (*E*) Integrated genome viewer (IGV) view of the *G0s2* gene CpG methylation of *Dnmt3a*^{WT} versus *Dnmt3a*^{KO} epidermal cells. Normalized methylated CpG reads are represented in bars (scale 0 to 1.0 for each row). Differentially methylated regions are indicated in the bottom track and highlighted in yellow.

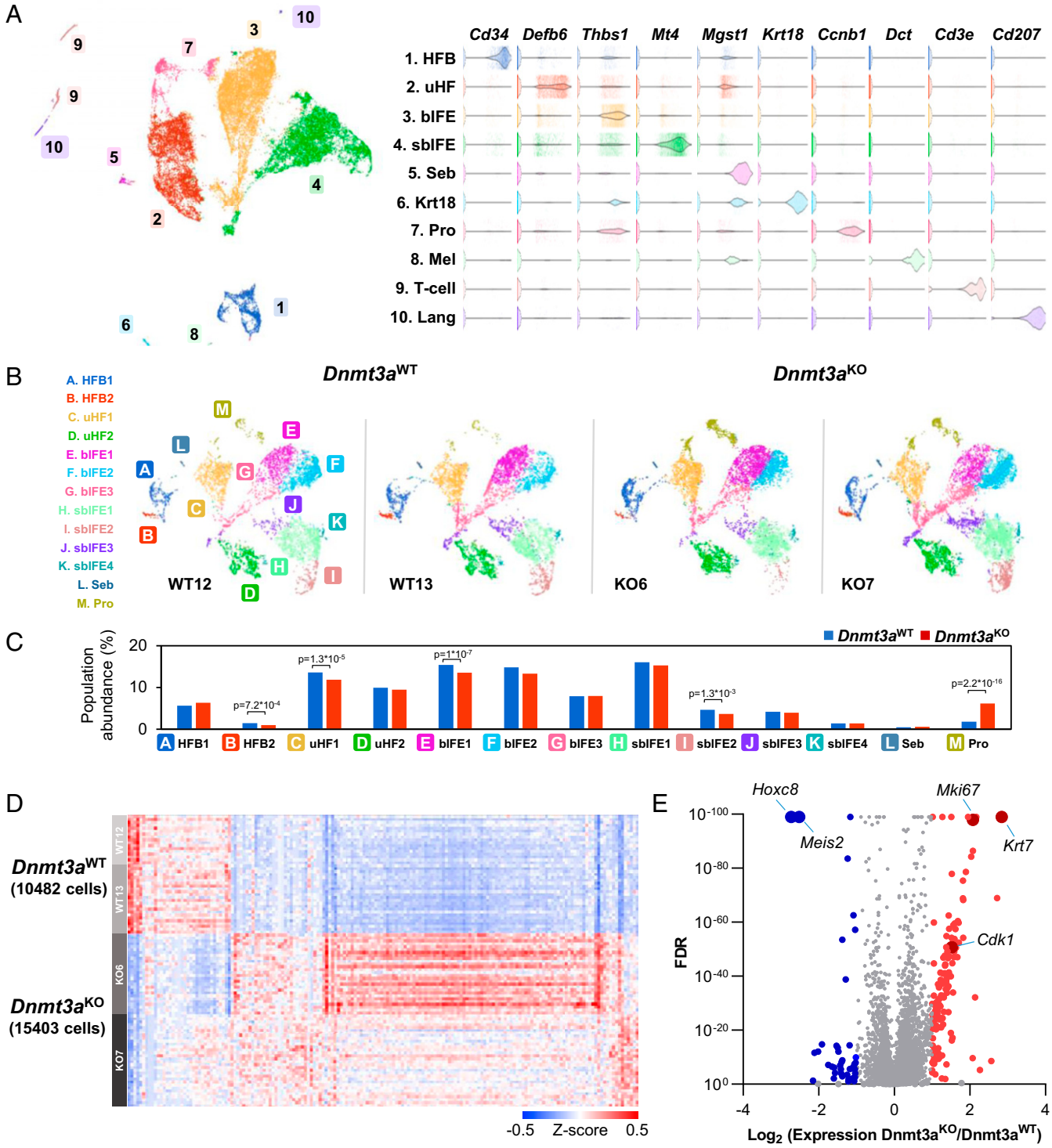

Fig. 2. Single-cell RNA sequencing reveals that Dnmt3a deficiency causes discrete gene expression changes in murine keratinocytes. (*A*) UMAP representation of single-cell RNA sequencing data from whole epidermis of two pairs of *Krt14*-Cre^{-} × *Dnmt3a*$^{fl/fl}$ (*Dnmt3a*^{WT}; 10,783 cells) and *Krt14*-Cre^{+} × *Dnmt3a*$^{fl/fl}$ mice (*Dnmt3a*^{KO};16,324 cells) with unbiased graph-based clustering demonstrating known skin populations represented by lineage defining genes (*Right*), including HFB, uHF, bIFE, sbIFE, and sebaceous gland (Seb), Krt18-expressing cells (Krt18), proliferative cells (Pro), melanocytes (Mel), T cells (T-cell), and Langerhan's cells (Lang). (*B*) Comparison of keratinocyte lineage cells in the *Dnmt3a*^{WT} versus *Dnmt3a*^{KO} mice, excluding inflammatory cells and melanocytes (excluded clusters 6, 8, 9, and 10). UMAP projections for each pair of samples with the indicated genotypes are shown. (*C*) No major population shifts are observed in epidermal lineages affected by *Krt14*-Cre mediated *Dnmt3a* deficiency, with the exception that the cells dominated by a proliferative signature (Pro, cluster M) are increased (6.1% in *Dnmt3a*^{KO} versus 1.8% in *Dnmt3a*^{WT}), as indicated by the bar graphs of keratinocyte lineage subclusters. Subclusters of the hair follicle bulge (A and B), upper hair follicle (C and D), basal interfollicular epidermis (E–G), suprabasal interfollicular epidermis (H–K), and sebocytes (L) are relatively unchanged. (*D*) Canonical gene expression changes were noted in single-cell RNA sequencing comparing keratinocyte lineage cells in *Dnmt3a*^{WT} versus *Dnmt3a*^{KO} epidermis (n = 2 mice per genotype). (*E*) There are 174 differentially expressed genes between *Dnmt3a*^{WT} and *Dnmt3a*^{KO} keratinocyte lineage cells with 137 up-regulated in the *Dnmt3a*^{KO} and 37 down-regulated genes with fold change >2 and FDR <0.01.

was dominated by expression of several genes associated with cellular proliferation ("Pro"), including genes encoding cyclins, cyclin-dependent kinases, and later cell cycle components like *Ube2c*, which encodes part of the anaphase promoting complex (see Fig. 4 below); this suggests that cells committed to mitosis have a signature dominated by components necessary for execution of the cell cycle (38).

The *Krt14*-Cre conditional knockout of *Dnmt3a* targets the epidermal keratinocyte lineages; we therefore excluded skin-infiltrating hematopoietic cells from subsequent analyses. Keratinocyte lineage UMAP representations of single-cell data demonstrate a high degree of similarity among samples, and unbiased clustering demonstrated similar distributions between populations (Fig. 2*B*, clusters A–M). Small, but statistically significant differences in population sizes between $Dnmt3a^{WT}$ and $Dnmt3a^{KO}$ epidermal keratinocytes were noted in the follicular bulge cluster 2 and upper hair follicle 1 (clusters B and C), as well as basal and suprabasal interfollicular epidermis (clusters E and I); however, the most dramatic difference was in the proliferative (Pro) cluster (cluster M), which is expanded 3.4-fold in $Dnmt3a^{KO}$ skin (1.8% vs. 6.1%, $P = 2.2*10^{-16}$, Fig. 2*C*). In addition to this population shift, there were canonical gene expression changes associated with *Dnmt3a* deficiency (Fig. 2*D*). In total, there were 174 differentially expressed genes (DEGs) exhibiting a fold change of 2 or greater with a FDR of 0.01 or less. Most of these genes (137) were more highly expressed in the $Dnmt3a^{KO}$ cells, while 37 were expressed at lower levels (Fig. 2 *D* and *E*).

Differentially Methylated Regions Are Associated with Gene Expression Changes. Of the 23,983 total DMRs identified by WGBS, 16,772 were within 10 kb of a gene, representing 5,573 unique genes. Of these, 2,181 genes (39%) were differentially expressed, as defined by an FDR of <0.01 and fold change >1, while 47 of these genes had an expression change of greater than twofold (38 up-regulated, and 9 down-regulated in $Dnmt3a^{KO}$ cells, Fig. 3*A*); however, the magnitude of methylation change was not predictive of expression changes. Further, some genes (e.g., *Krt7* and *Meis2*) exhibited dramatic but opposing expression changes, despite associated DMRs that were hypomethylated to a similar extent (Fig. 3*B*). The location of DMRs within annotated regions (e.g., enhancers, CpG islands, etc.) did not predict the magnitude or direction of expression changes (*SI Appendix*, Fig. S2).

Meis2 is a homeobox transcription factor involved in developmental processes and regulation of tumor proliferation (39), and *Hoxc8* modulates Wnt signaling in the hair follicle niche to control hair follicle regeneration (40). Both are DMR-associated genes and are expressed at significantly lower levels in most $Dnmt3a^{KO}$ epidermal cells (Fig. 3 *C* and *D* and *SI Appendix*, Fig. S3*A*), suggesting that the normal expression of these two genes may be linked to DNA methylation marks added by Dnmt3a. In contrast, some genes are differentially expressed only in subpopulations of skin cells. For example, Keratin 7 (*Krt7*), which is frequently overexpressed in aggressive subtypes of cutaneous squamous cell carcinoma, and associated with poor survival in patients with esophageal squamous cell carcinoma (41, 42), is predominantly expressed in the upper hair follicle in $Dnmt3a^{WT}$ mice; in $Dnmt3a^{KO}$ mice, its expression increases in the upper hair follicle as well as the basal and suprabasal interfollicular epidermis compartments (Fig. 3*E* and *SI Appendix*, Fig. S3*B*). Similarly, *Irx1* is primarily expressed in the hair follicle bulge and upper hair follicle cells of $Dnmt3a^{WT}$ mice, but its expression increases in all compartments in $Dnmt3a^{KO}$ mice (Fig. 3*F* and *SI Appendix*, Fig. S3*B*), a finding that was validated by Western blotting (Fig. 3*G*). Decreased methylation in the *IRX1* promoter is associated with increased expression and metastatic capability in osteosarcoma (43).

Deficiency in Dnmt3a Is Associated with an Increased Fraction of Cycling Cells in the Skin. The most significant population shift between $Dnmt3a^{WT}$ and $Dnmt3a^{KO}$ keratinocyte lineage cells occurred in a cluster that was dominated by the expression of genes associated with cell division (Figs. 2 *B* and *C* and 4*A*). This population (cluster M) was defined by the expression of late interphase cyclins (e.g., *Ccna2* and *Ccnb2*), as well as later cell cycle genes like *Cenpf*; these genes are rarely expressed in the cells of any other clusters (Fig. 4*B*). The size of this "proliferative cluster" expanded from 1.8% of total epidermal cells in $Dnmt3a^{WT}$ mice to 6.1% in $Dnmt3a^{KO}$ mice (3.4-fold, Fig. 4*A*), similar to the increase in the fraction of cells expressing *Mki67* (from 2.8 to 10.2%, 3.6-fold, Fig. 4*C*). The expression of cell cycle genes in cluster M was equally high in $Dnmt3a^{WT}$ and $Dnmt3a^{KO}$ cells, as expected, since all cells in this cluster are likely to be actively dividing, regardless of their genotype (Fig. 4*D*); however, $Dnmt3a^{KO}$ cells in clusters A–L demonstrated increased expression levels of cell cycle genes, including *Mki67* (although the expression levels of these genes were far lower than that of proliferating cells), as well as the essential cyclin-dependent kinase *Cdk1*, which is a differentially expressed gene associated with a DMR (Fig. 3*A*). To validate the proliferative phenotype with an orthogonal method, we injected 5-bromo-2′-deoxyuridine (BrdU) intraperitoneally into young (8 to 9 wk old) $Dnmt3a^{WT}$ and $Dnmt3a^{KO}$ mice, and generated single-cell suspensions of epidermal cells 24 h later for flow cytometric analysis of BrdU uptake. As predicted by the single-cell RNA-sequencing (scRNA-seq) data, the fraction of actively cycling, Cd45-negative epidermal cells was significantly increased in the $Dnmt3a^{KO}$ mice (Fig. 4*E*). Epidermal subpopulations likewise demonstrated significantly increased BrdU incorporation in $Dnmt3a^{KO}$ basal interfollicular epidermis cells (and trended upwards in the upper hair follicle); however, no change was detected in the follicular bulge stem cell compartment, or the postmitotic suprabasal interfollicular epidermis, neither of which proliferates in the telogen state (*SI Appendix*, Fig. S4 *A* and *B*).

Focal, Canonical DNA Hypomethylation in the Skin of a Patient with a Dominant-Negative *DNMT3A*^{R882H} Mutation. Patients with TBRS have germline mutations in *DNMT3A* and exhibit several common clinical features, including overgrowth, characteristic facies, and neuropsychiatric disorders (44, 45), as well as an increased risk of developing AML and perhaps other malignancies. We previously demonstrated that the peripheral blood cells from a nonleukemic patient with a heterozygous germline $DNMT3A^{R882H}$ allele exhibited a focal, canonical hypomethylation phenotype similar to that of AML samples initiated by the same mutation, suggesting that hypomethylation precedes transformation (30).

To determine whether this mutation causes a methylation phenotype in human skin, we analyzed DNA methylation in two skin samples from the same TBRS patient (at ages 9 and 14) and his unaffected brother (at ages 13 and 17). Global DNA methylation levels were minimally altered (similar to $Dnmt3a^{KO}$ skin). Nearly all of the 1,234 DMRs identified (1,221/1,234; 98.9%) were hypomethylated (Fig. 5*B*); the smaller number of DMRs (compared to $Dnmt3a^{KO}$ mouse skin) probably reflects the fact that the R882H mutation is dominant negative (80% reduced activity) rather than null, and also the reduced power to detect DMRs with only two samples from each genotype. Plotting the mean methylation values of each DMR between both samples from the two brothers demonstrated the canonical nature of most of these DMRs (Fig. 5*C*). These DMRs were most likely to occur in gene bodies, similar to that seen in $Dnmt3a^{KO}$ mice (Figs. 1*D* and 5*E*).

At many loci, there was a striking similarity in DNA methylation patterns between the DMRs of homologous genes in mice and humans. For example, DMRs near the homeobox gene *IRX3* in human TBRS skin are similar to DMRs near *Irx3* in mouse skin (Fig. 5 *D*, *Left*). Another gene important for development, *FZD1*, shares a similar methylation phenotype between the TBRS

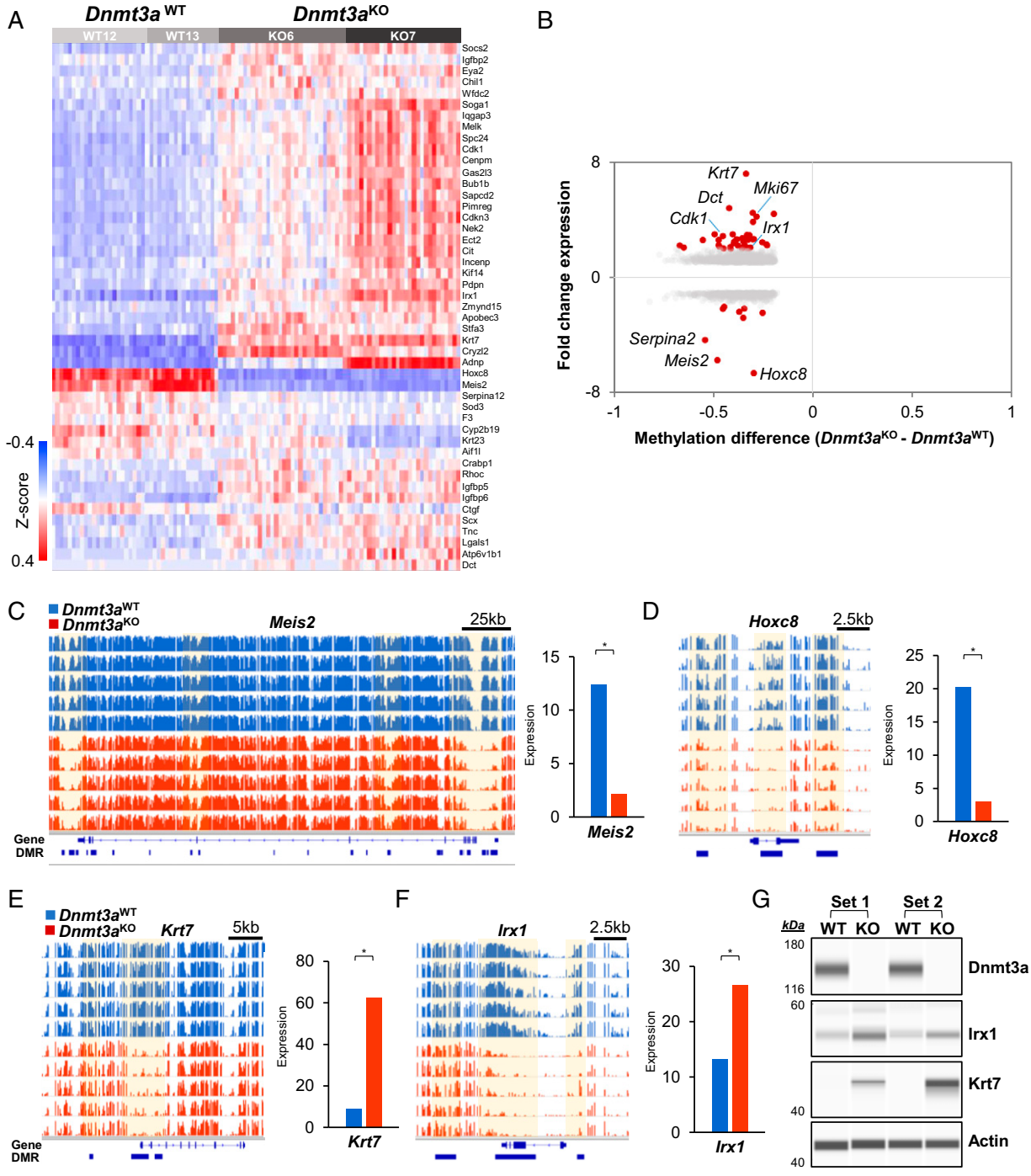

Fig. 3. Differentially methylated regions are associated with differentially expressed genes. (*A*) Heatmap from single-cell RNA sequencing represents the 47 differentially expressed genes between *Dnmt3a*^{WT} and *Dnmt3a*^{KO} keratinocyte lineage cells that are associated with a *Dnmt3a* DMR and exhibit an expression fold change >2 with an FDR <0.01. Grayscale bars represent cells from independent samples, two from each genotype. (*B*) Relationship between gene expression and methylation changes between *Dnmt3a*^{KO} and *Dnmt3a*^{WT} keratinocytes. There are 5,968 differentially expressed genes with an FDR <0.01, of these there are 2,181 genes associated with DMRs. This plot represents expression versus methylation of these 2,181 genes. Significant differential expression, with fold change >2 denoted as red dots. Gray dots represent fold change between 1 and 2. (*C*) IGV views of differentially methylated regions associated with *Meis2*, which has annotated DMRs in CpG islands, shelves, shores, and gene body. Gene expression of *Meis2* changes by −5.77-fold (FDR $5.7*10^{-249}$). *Dnmt3a*^{KO} expresses *Meis2* in 172/15,403 (1.11%) of cells compared to *Dnmt3a*^{WT} 1,106/10,482 (10.6%). (*D*) Differentially methylated regions associated with *Hoxc8*, which has DMRs in shores and gene body. *Hoxc8* expression changes by −6.72-fold (FDR $2.51*10^{-300}$) and is expressed in 234/15,403 (1.52%) *Dnmt3a*^{KO} cells compared to 1,375/10,482 (13.1%) *Dnmt3a*^{WT}. (*E*) Differentially methylated regions associated with *Krt7*, which has DMRs in shores, shelves, promoter, and gene body. Expression is changed by 7.19-fold in *Dnmt3a*^{KO} (FDR $9.2*10^{-182}$), and cells expressing increase to *Dnmt3a*^{KO} 2,551/15,403 (16.6%) from *Dnmt3a*^{WT} 573/10,482 (5.47%). (*F*) Differentially methylated regions associated with *Irx1*, which has DMRs in CpG islands, shores, promoter, and gene body. Expression is changed by 2.02-fold (FDR $1.16*10^{-109}$) in *Dnmt3a*^{KO} keratinocyte lineage cells, and cells expressing increases from 2,873/15,403 (18.7%) *Dnmt3a*^{KO} cells to 885/10,482 (8.44%) *Dnmt3a*^{WT}. (*G*) Simple Western demonstrates protein level expression changes in Irx1 and Krt7 from epidermal cells isolated from the indicated *Dnmt3a*^{WT} and *Dnmt3a*^{KO} littermates (bracketed). Actin serves as a loading control.

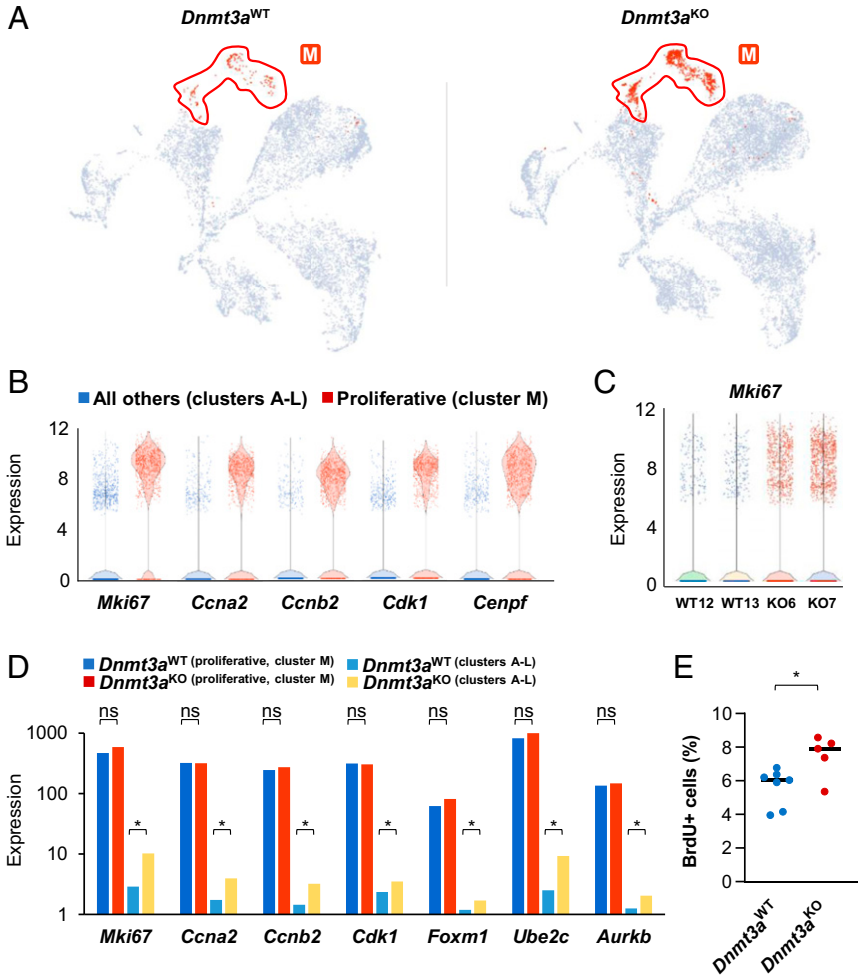

Fig. 4. Dnmt3a-deficient keratinocytes exhibit a proliferative phenotype. (*A*) UMAP of *Dnmt3a*^{WT} and *Dnmt3a*^{KO} single-cell RNA sequencing data representing a pair of samples for each indicated genotype, highlighting the population (in red) identified by unbiased clustering as dominated by expression of genes involved in cell cycling (cluster M). (*B*) Proliferative gene expression in the proliferative cluster (cluster M) versus the aggregate of the remaining keratinocyte linage clusters (clusters A–L). These data represent the aggregate of *Dnmt3a*^{WT} and *Dnmt3a*^{KO} cells. Each dot is an individual cell. Expression values are represented by least-squares (LS) means. (*C*) The number of cells expressing the proliferative marker gene *Mki67* increases from 298/10,485 (2.8%) cells in *Dnmt3a*^{WT} to 1,509/14,815 (10.2%) cells in the *Dnmt3a*^{KO}. (*D*) Single-cell RNA-sequencing expression data of multiple cell cycle relevant genes, comparing the proliferative cells (cluster M) versus the rest (cluster A–L). *FDR <0.01 and ns, not significant. Expression values are represented by LS means. (*E*) BrdU uptake in vivo in keratinocytes assessed by flow cytometry (Cd45-negative, single-cell epidermal suspension) comparing *Dnmt3a*^{WT} ($n = 7$) and *Dnmt3a*^{KO} ($n = 5$) mice injected 24 h earlier with BrdU. BrdU uptake is significantly higher in *Dnmt3a*^{KO} epidermal keratinocytes (5.6% BrdU+ in *Dnmt3a*^{WT} vs. 7.5% BrdU+ in *Dnmt3a*^{KO}, $P = 0.023$).

skin and mouse *Dnmt3a*^{KO} skin (Fig. 5 *D*, *Right*). The Wnt signaling pathway is important both for skin and bone development, and multiple genes of the Wnt pathway also exhibited similar Dnmt3a-dependent methylation patterns between mouse and human skin (*SI Appendix*, Fig. S5). Of the 1,034 DMR-associated genes identified in the TBRS patient, 432 overlapped with *Dnmt3a*^{KO} DMR-associated genes identified in mouse skin (Fig. 5*F*).

Discussion

The purpose of this study was to define the baseline epigenetic characteristics of Dnmt3a-deficient skin. Using WGBS, we defined the focal, canonical DNA methylation phenotype of Dnmt3a-deficient mouse epidermal cells and of a human patient with a germline *DNMT3A*^{R882H} mutation. The small changes in the global methylation state of epidermal cells reflects the restricted places in the genome where Dnmt3a acts, and the small sizes of these regions (on average, less than 1 Kb). There were 1,234 DMRs identified in the skin of the TBRS patient, which affected 3.19% of annotated gene bodies. Similarly, Dnmt3a-dependent methylation in murine epidermis occurred most often in gene bodies—more than in promoters or CpG island shores, which were the next most common regions affected. However, the magnitude and location of these differentially methylated regions were not predictive of gene expression changes detected by scRNA-seq. Overall, there were 5,968 DEGs in *Dnmt3a*^{KO} skin cells, but the number of DEGs that were close to a DMR (i.e., within 10 Kb) represented a subset of these genes (2,181/5,968; 36.5%). Only a small subset of these exhibited an expression fold change of >2 (2.15% of DMR associated DEGs, 0.8% of all DEGs). Like multiple previous studies (18, 30, 46), the relationship of DMRs to gene expression patterns was unpredictable at a global level, again demonstrating that DNA methylation is but one factor in determining the expression of a specific gene in a specific cellular context. Prior studies demonstrated accurate remethylation of Dnmt3a-dependent DMRs in *Dnmt3a*^{KO} bone marrow with induced expression of wild-type DNMT3A, as well as correction of a subset of gene expression changes (18). However, it is not yet clear whether remethylation was directly responsible for altering the expression of these differentially expressed genes.

Aging and sun exposure have been demonstrated to cause DNA methylation changes, which were particularly apparent comparing

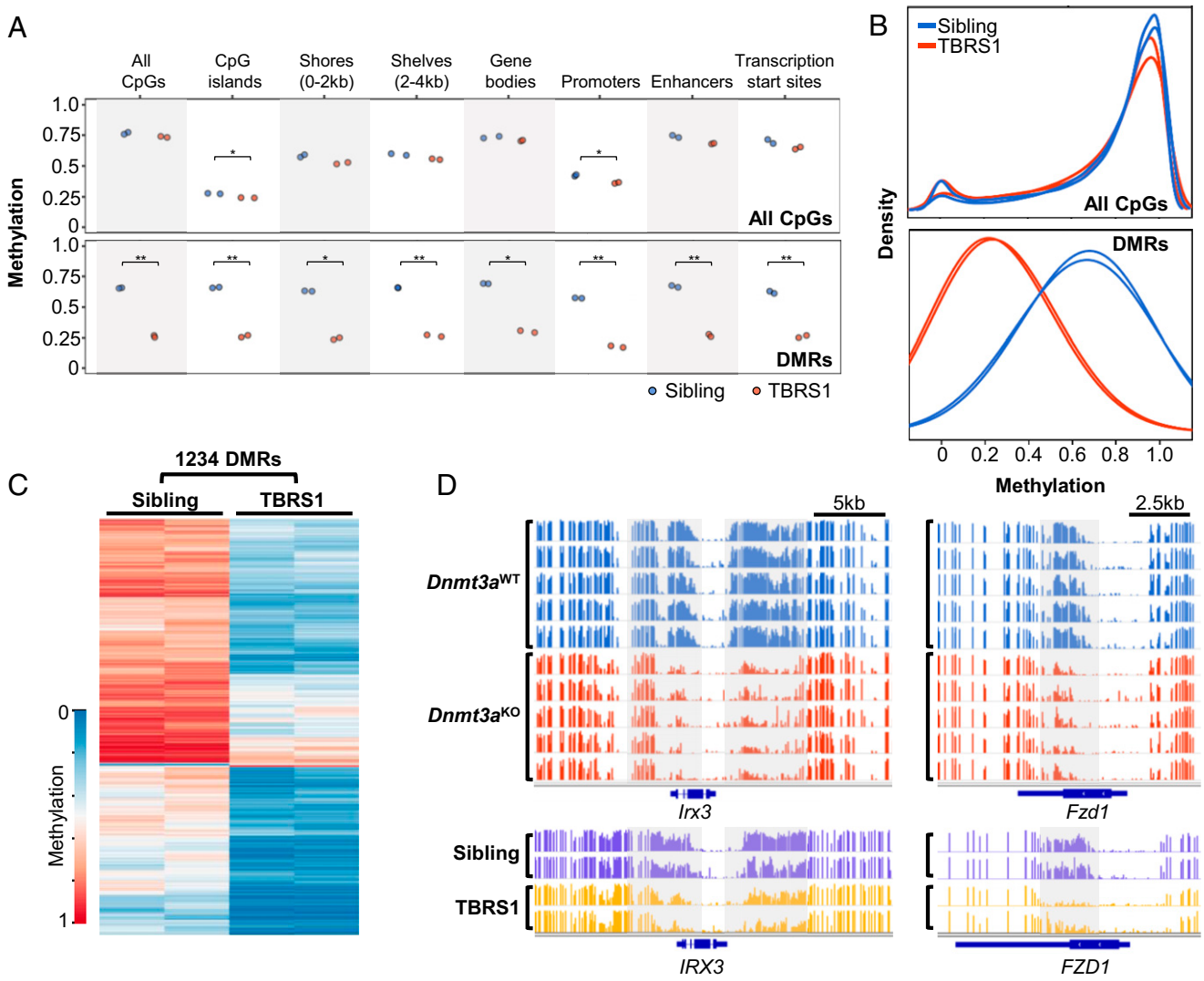

E

	Total	DMRs	% Total
CpG island	31144	640	2.05
Shore	56324	391	0.69
Shelf	78636	57	0.07
Gene body	19951	637*	3.19*
Promoter	38459	185	0.48
Enhancer	121622	13	0.01
TSS	28988	29	0.10

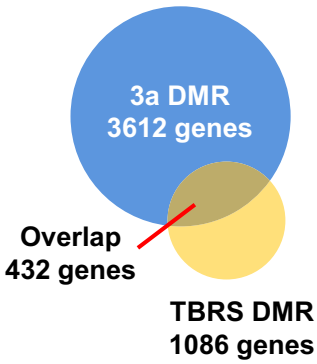

Fig. 5. A germline, dominant-negative *DNMT3A* mutation causes focal DNA methylation alterations in human skin. (*A*) Whole genome bisulfite sequencing analysis for whole skin samples comparing two samples from a TBRS patient and his brother, comparing CpG methylation globally (*Top*) or at DMRs (*Bottom*). Level of significance * adjusted $P < 0.05$ and ** $P < 0.01$. (*B*) Density plots demonstrate global CpG methylation (*Top*) and CpG methylation at DMRs (*Bottom*) in the TBRS patient and his unaffected sibling. (*C*) Heatmap illustrates 1,234 differentially methylated regions in the skin of the TBRS patient, compared with his sibling. (*D*) IGV visualization of CpG methylation at the *IRX3*/*Irx3* and *FZD1*/*Fzd1* loci. Each row represents an independent sample with *Dnmt3a*^{WT} vs. *Dnmt3a*^{KO} represented in blue and red (*Top*) and sibling vs. TBRS patient in purple and yellow (*Bottom*). Gray boxes highlight areas of differential methylation. (*E*) Gene bodies are the most frequently involved annotated region by TBRS DMRs. *There are 963 DMRs that reside in annotated gene bodies, representing 637 unique genes. (*F*) There are 23,983 DMRs in the *Dnmt3a*^{KO}, 16,315 of them are within 10 kb of 3,612 unique genes. Of the 1,234 TBRS DMRs, 1,086 are located within 10 kb of genes in the human genome. Of the 1,086 TBRS-DMR associated genes, 707 have a mouse homolog, with 432 genes overlapping DMR-associated genes in *Dnmt3a*^{KO} mice and the TBRS patient.

UV-exposed skin in older patients to UV-protected skin in younger patients. Large, predominantly hypomethylated blocks were found to cover 99 Mb of the genome in older, UV-exposed skin (5). Although the cause of this phenotype is unknown, a number of possibilities exist, including a progressive decline in expression (or function) of the DNA methyltransferases, or increased activity of the demethylases (i.e., *TET* gene family members). In mice, *Dnmt1* and *Dnmt3a* are expressed in the basal layer of keratinocytes during development; however, in adults, the expression of Dnmt1 is restricted to the hair follicle, and *Dnmt3a* expression is restricted to the interfollicular epidermis (8, 11). Notably, Dnmt3a expression decreases in this compartment in adult mice (11), though it is not yet clear whether these findings contribute to the increased risk of skin cancers in elderly patients.

To begin to address this question, Rinaldi et al. demonstrated that epidermal Dnmt3a deficiency resulted in decreased tumor latency and increased tumor numbers in mouse skin treated with DMBA/TPA, suggesting that the threshold for oncogenic transformation is lower in mice with *Dnmt3a* deficiency (11). In the same study, mice with Dnmt3b deficiency had no phenotype, and compound deficiency of Dnmt3a and Dnmt3b (double knockout/DKO) resulted in tumor latency that was indistinguishable from that of Dnmt3a deficiency; however, a broader spectrum of tumors arose in the DKO mice, including basal cell carcinomas, as well as more aggressive tumors (including squamous cell and spindle cell carcinomas). These tumors developed a reliance on *Pparg*; we did not detect up-regulation of *Pparg* in the premalignant state, suggesting that dysregulation may occur during or after transformation. In contrast, certain gene expression changes (i.e., increased expression of *G0s2*) persisted from the Dnmt3a-deficient preneoplastic state to the resulting tumors (11) (Fig. 1*E* and Dataset S2). Together, these data strongly suggested that Dnmt3a deficiency creates a premalignant state for keratinocyte carcinomas in mice, with some gene expression changes that persist in tumors. We observed that Dnmt3b deficiency causes only 20 DMRs in the skin, and that Dnmt3a and Dnmt3b compound deficiency (DKO) adds little to the $Dnmt3a^{KO}$ methylation phenotype (*SI Appendix*, Fig. S6). Therefore, in mouse skin, Dnmt3a is the dominant de novo DNA methyltransferase, and the loss of its function in aging skin could likewise be relevant for human skin cancer pathogenesis.

Although Dnmt3a deficiency results in minimal skin population changes, it is associated with an expanded number of cells with a proliferative signature in the $Dnmt3a^{KO}$ epidermis. Despite this, the skin of young mice is not measurably thickened, and spontaneous skin cancers do not occur, suggesting that robust compensatory mechanisms are active. Multiple critical cell cycle genes, including *Ccna2* or *Cdk1*, are up-regulated in both proliferating and nonproliferating cells as well; conversely, the cyclin-dependent kinase inhibitor *Cdkn1a* is down-regulated in nonproliferating Dnmt3a-deficient cells (*SI Appendix*, Fig. S7*A*). The expression of *Mki67* is tightly regulated and absent in quiescent (G0) cells and more highly expressed in G2 through M phase cells. Cells that are more frequently in the cell cycle express higher levels of *Mki67* than quiescent cells (47). Indeed, we found that *Mki67* expression is elevated even in the nonproliferating cells of $Dnmt3a^{KO}$ mice, which may reflect the proliferative history of these cells. Together, these results suggest that Dnmt3a deficiency may prime epidermal keratinocytes to enter the cell cycle, or remove antiproliferative "brakes" from mitogenic signals. While proliferative signaling was implicated, *Cdk1* was the only direct proliferative driver associated with a DMR and expressed with a fold change >2.

Enhanced proliferation has been observed in the setting of DNMT3A deficiency in other premalignant and malignant conditions. Decreased *DNMT3A* expression has been associated with nonmalignant adenomyosis, where ectopic endometrial cells invade the myometrium. These cells exhibit increased proliferation with *DNMT3A* knockdown, and decreased proliferation with overexpression (48). Additionally, a model of Dnmt3a deficiency in $KRAS^{G12D}$ driven lung tumors demonstrated that at 24 wk after induction, $Dnmt3a^{KO}$ tumors were six times larger than their $Dnmt3a^{WT}$ counterparts and exhibited a markedly higher proliferative index (49). Together, these findings suggest that epigenetic changes caused by Dnmt3a deficiency can result in a hyperproliferative state in several cellular contexts. The specific genes responsible for initiating this phenotype are not yet clear, but several good candidates (i.e., *Cdk1*, *Hras*, *E2f1*, and *Cdkn1a*) are defined in this study (*SI Appendix*, Fig. S7 *B–D*). Proliferative priming may therefore represent one mechanism that is relevant for the premalignant state associated with DNMT3A haploinsufficiency or deficiency in multiple tissues. The resulting expanded proliferative capacity may exist in equilibrium until cooperating mutations occur, which appear to be essential for transformation in many model systems.

In addition to clonal hematopoiesis, premalignant mutation-driven clonal expansion has now been shown to occur in many other systems, including the skin (2), liver (50), esophagus (51, 52), and bronchial epithelium (53). Mutationally driven, expanded clones usually do not progress to frank malignancies, suggesting that additional epigenetic or genetic alterations are required to cause transformation. In clonal hematopoiesis, the expansion of hematopoietic stem/progenitor cells is usually caused by mutations in epigenetic regulatory genes, most commonly in *DNMT3A* (23, 24, 26, 54). These clonally expanded cells are at increased risk of transformation to myelodysplastic syndromes or AML, likely by altering the epigenetic "fitness" of these cells for transformation (55–57). Similar epigenetic fitness alterations may modify tumor susceptibility in skin and other organs by a variety of mechanisms.

We identified similarities between the methylation phenotypes of mice and humans with decreased DNMT3A activity: DMRs in the epidermis of $Dnmt3a^{KO}$ mice shared considerable gene-level similarity with a TBRS patient with a germline $DNMT3A^{R882H}$ mutation. In fact, 432 out of the 1,086 gene-associated DMRs identified in the skin of this patient overlapped with gene-associated DMRs found in $Dnmt3a^{KO}$ skin. Several of these overlapping genes have known roles in development, including *IRX3*/*Irx3*; this locus shares a high degree of evolutionary conservation in noncoding sequences between human, mouse, and zebrafish, suggesting the presence and conservation of both functional and regulatory elements (58). Additionally, important pathways in skin development (like the WNT pathway) have multiple members with similar *DNMT3A*/*Dnmt3a*-dependent methylation patterns (*SI Appendix*, Fig. S5). Recent descriptions of AMLs and central nervous system (CNS) tumors in young patients with germline loss-of-function *DNMT3A* mutations strongly suggest that DNMT3A acts as a tumor suppressor in both hematopoietic and CNS cells (59). Although the skin phenotype and skin cancer susceptibility of children with TBRS has not yet been described, our data suggest that these patients may be at elevated risk, and that appropriate primary prevention measures should be taken to protect these patients from sustained UV light exposure. Finally, these data also suggest a role for *DNMT3A* in keratinocyte carcinomas arising in aging and sun-exposed skin; additional studies to define this role are in progress.

Materials and Methods

Human Studies. Samples were obtained as part of a study approved by the Human Research Protection Office at Washington University School of Medicine (approval #201011766), which explicitly allows for potentially identifying genomic studies, including whole genome sequencing. Written informed consent was obtained from the parents of the patient with TBRS (and his unaffected brother) for whole genome bisulfite sequencing studies, in accordance with the institutional review board approved protocol at Washington University School of Medicine.

Animals and Epidermal Cell Isolation. All mouse work was performed in accordance with institutional guidelines and approved by the Animal Studies Committee at Washington University. For all studies, we harvested single-cell suspensions of dorsal epidermis in second telogen (7 to 10 wk of age), or in

older mice, when skin is >90% telogen based on pale or pink skin color. Details for mouse strain and epidermal single-cell suspensions can be found in *SI Appendix, Supplementary Materials and Methods*.

Whole Genome Bisulfite Sequencing and Analysis. WGBS was performed as described previously (17) with the exception that DNA was generated from epidermal cells. Alignment and DMR calling details are in *SI Appendix, Supplementary Materials and Methods*.

Single-Cell RNA Sequencing and Analysis. Single-cell suspensions of murine epidermis were freshly prepared and libraries generated using the 10× Chromium Controller system. Data analysis was performed using the standard tools available in the Partek Flow software suite (Partek, Inc.). Full details of the analysis are in *SI Appendix, Supplementary Materials and Methods*.

Immunoblotting and Flow Cytometry. Freshly isolated single-cell suspensions of murine epidermis were lysed in radioimmunoprecipitation assay (RIPA) buffer or suspended in staining buffer for further analysis by flow cytometry. Lysis and staining conditions (as well as antibody information) are described in *SI Appendix, Supplementary Materials and Methods*.

Data Availability. DNA and RNA sequences (mouse data) have been deposited in NCBI Sequence Read Archive (BioProject PRJNA674614). Anonymized DNA sequences (human data) have been deposited in dbGaP (https://www.ncbi.nlm.nih.gov/projects/gap/cgi-bin/study.cgi?study_id=phs000159.v10.p5).

ACKNOWLEDGMENTS. This study was supported by grants from the Dermatology Foundation (Dermatologist Investigator Research Fellowship and Physician Scientist Career Development Award) and NIH Grants CA237727 (to D.Y.C.), CA211782 (to C.A.M.), and CA101937 and CA197561, and a Barnes Jewish Foundation Award #5169 (to T.J.L.). The Siteman Cancer Center Flow Cytometry Core (National Cancer Institute P30CA91842) provided expert support for all flow sorting studies. We thank Mieke Hoock for excellent animal husbandry.

1. H. W. Rogers, M. A. Weinstock, S. R. Feldman, B. M. Coldiron, Incidence estimate of nonmelanoma skin cancer (keratinocyte carcinomas) in the U.S. Population, 2012. *JAMA Dermatol.* **151**, 1081–1086 (2015).
2. I. Martincorena *et al*., Tumor evolution. High burden and pervasive positive selection of somatic mutations in normal human skin. *Science* **348**, 880–886 (2015).
3. S. Baylin, T. H. Bestor, Altered methylation patterns in cancer cell genomes: Cause or consequence? *Cancer Cell* **1**, 299–305 (2002).
4. W. Timp, A. P. Feinberg, Cancer as a dysregulated epigenome allowing cellular growth advantage at the expense of the host. *Nat. Rev. Cancer* **13**, 497–510 (2013).
5. A. R. Vandiver *et al*., Age and sun exposure-related widespread genomic blocks of hypomethylation in nonmalignant skin. *Genome Biol.* **16**, 80 (2015).
6. T. Chen, Y. Ueda, J. E. Dodge, Z. Wang, E. Li, Establishment and maintenance of genomic methylation patterns in mouse embryonic stem cells by Dnmt3a and Dnmt3b. *Mol. Cell. Biol.* **23**, 5594–5605 (2003).
7. P. A. Jones, G. Liang, Rethinking how DNA methylation patterns are maintained. *Nat. Rev. Genet.* **10**, 805–811 (2009).
8. J. Li *et al*., Progressive alopecia reveals decreasing stem cell activation probability during aging of mice with epidermal deletion of DNA methyltransferase 1. *J. Invest. Dermatol.* **132**, 2681–2690 (2012). Corrected in: *J. Invest. Dermatol.* **133**, 859 (2013).
9. G. L. Sen, J. A. Reuter, D. E. Webster, L. Zhu, P. A. Khavari, DNMT1 maintains progenitor function in self-renewing somatic tissue. *Nature* **463**, 563–567 (2010).
10. L. Rinaldi *et al*., Dnmt3a and Dnmt3b associate with enhancers to regulate human epidermal stem cell homeostasis. *Cell Stem Cell* **19**, 491–501 (2016).
11. L. Rinaldi *et al*., Loss of Dnmt3a and Dnmt3b does not affect epidermal homeostasis but promotes squamous transformation through PPAR-γ. *eLife* **6**, e21697 (2017).
12. M. Rodríguez-Paredes *et al*., Methylation profiling identifies two subclasses of squamous cell carcinoma related to distinct cells of origin. *Nat. Commun.* **9**, 577 (2018).
13. C. R. Pickering *et al*., Mutational landscape of aggressive cutaneous squamous cell carcinoma. *Clin. Cancer Res.* **20**, 6582–6592 (2014).
14. Y. Y. Li *et al*., Genomic analysis of metastatic cutaneous squamous cell carcinoma. *Clin. Cancer Res.* **21**, 1447–1456 (2015).
15. X. Bonilla *et al*., Genomic analysis identifies new drivers and progression pathways in skin basal cell carcinoma. *Nat. Genet.* **48**, 398–406 (2016).
16. M. Jeong *et al*., Large conserved domains of low DNA methylation maintained by Dnmt3a. *Nat. Genet.* **46**, 17–23 (2014).
17. C. B. Cole *et al*., Haploinsufficiency for DNA methyltransferase 3A predisposes hematopoietic cells to myeloid malignancies. *J. Clin. Invest.* **127**, 3657–3674 (2017).
18. S. Ketkar *et al*., Remethylation of *Dnmt3a*$^{-/-}$ hematopoietic cells is associated with partial correction of gene dysregulation and reduced myeloid skewing. *Proc. Natl. Acad. Sci. U.S.A.* **117**, 3123–3134 (2020).
19. A. Mayle *et al*., Dnmt3a loss predisposes murine hematopoietic stem cells to malignant transformation. *Blood* **125**, 629–638 (2015).
20. H. Celik *et al*., Enforced differentiation of Dnmt3a-null bone marrow leads to failure with c-Kit mutations driving leukemic transformation. *Blood* **125**, 619–628 (2015).
21. I. H. I. M. Hollink *et al*., Acute myeloid leukaemia in a case with Tatton-Brown-rahman syndrome: The peculiar *DNMT3A* R882 mutation. *J. Med. Genet.* **54**, 805–808 (2017).
22. R. Kosaki, H. Terashima, M. Kubota, K. Kosaki, Acute myeloid leukemia-associated DNMT3A p.Arg882His mutation in a patient with Tatton-Brown-Rahman overgrowth syndrome as a constitutional mutation. *Am. J. Med. Genet. A.* **173**, 250–253 (2017).
23. M. Xie *et al*., Age-related mutations associated with clonal hematopoietic expansion and malignancies. *Nat. Med.* **20**, 1472–1478 (2014).
24. S. Jaiswal *et al*., Age-related clonal hematopoiesis associated with adverse outcomes. *N. Engl. J. Med.* **371**, 2488–2498 (2014).
25. G. Genovese *et al*., Clonal hematopoiesis and blood-cancer risk inferred from blood DNA sequence. *N. Engl. J. Med.* **371**, 2477–2487 (2014).
26. A. G. Bick *et al*.; NHLBI Trans-Omics for Precision Medicine Consortium, Inherited causes of clonal haematopoiesis in 97,691 whole genomes. *Nature* **586**, 763–768 (2020).
27. T. J. Ley *et al*., DNMT3A mutations in acute myeloid leukemia. *N. Engl. J. Med.* **363**, 2424–2433 (2010).
28. M. Okano, D. W. Bell, D. A. Haber, E. Li, DNA methyltransferases Dnmt3a and Dnmt3b are essential for de novo methylation and mammalian development. *Cell* **99**, 247–257 (1999).
29. H. R. Dassule, P. Lewis, M. Bei, R. Maas, A. P. McMahon, Sonic hedgehog regulates growth and morphogenesis of the tooth. *Development* **127**, 4775–4785 (2000).
30. D. H. Spencer *et al*., CpG island hypermethylation mediated by DNMT3A is a consequence of AML progression. *Cell* **168**, 801–816.e13 (2017).
31. D. M. Jeziorska *et al*., DNA methylation of intragenic CpG islands depends on their transcriptional activity during differentiation and disease. *Proc. Natl. Acad. Sci. U.S.A.* **114**, E7526–E7535 (2017).
32. E. Becht *et al*., Dimensionality reduction for visualizing single-cell data using UMAP. *Nat. Biotechnol.* **37**, 38–44 (2018).
33. C. S. Trempus *et al*., Enrichment for living murine keratinocytes from the hair follicle bulge with the cell surface marker CD34. *J. Invest. Dermatol.* **120**, 501–511 (2003).
34. S. Joost *et al*., Single-cell transcriptomics reveals that differentiation and spatial signatures shape epidermal and hair follicle heterogeneity. *Cell Syst.* **3**, 221–237.e9 (2016).
35. A. Füllgrabe *et al*., Dynamics of Lgr6^{+} progenitor cells in the hair follicle, sebaceous gland, and interfollicular epidermis. *Stem Cell Reports* **5**, 843–855 (2015).
36. C. Blanpain, E. Fuchs, Epidermal homeostasis: A balancing act of stem cells in the skin. *Nat. Rev. Mol. Cell Biol.* **10**, 207–217 (2009).
37. J. Varani *et al*., Thrombospondin-induced adhesion of human keratinocytes. *J. Clin. Invest.* **81**, 1537–1544 (1988).
38. M. L. Whitfield *et al*., Identification of genes periodically expressed in the human cell cycle and their expression in tumors. *Mol. Biol. Cell* **13**, 1977–2000 (2002).
39. A. Groß *et al*., Tumorigenic and anti-proliferative properties of the TALE-transcription factors MEIS2D and MEIS2A in neuroblastoma. *Cancer Res.* **78**, 1935–1947 (2018).
40. Z. Yu *et al*., Hoxc-dependent mesenchymal niche heterogeneity drives regional hair follicle regeneration. *Cell Stem Cell* **23**, 487–500.e6 (2018).
41. M. Pulitzer, G. Desman, K. J. Busam, CK7 expression in primary cutaneous squamous cell carcinoma. *J. Cutan. Pathol.* **37**, 966–972 (2010).
42. A. Yamada *et al*., Expression of cytokeratin 7 predicts survival in stage I/IIA/IIB squamous cell carcinoma of the esophagus. *Oncol. Rep.* **20**, 1021–1027 (2008).
43. J. Lu *et al*., IRX1 hypomethylation promotes osteosarcoma metastasis via induction of CXCL14/NF-κB signaling. *J. Clin. Invest.* **125**, 1839–1856 (2015).
44. K. Tatton-Brown *et al*.; Childhood Overgrowth Consortium, Mutations in the DNA methyltransferase gene DNMT3A cause an overgrowth syndrome with intellectual disability. *Nat. Genet.* **46**, 385–388 (2014).
45. W. Shen *et al*., The spectrum of DNMT3A variants in Tatton-Brown-Rahman syndrome overlaps with that in hematologic malignancies. *Am. J. Med. Genet. A.* **173**, 3022–3028 (2017).
46. D. A. Russler-Germain *et al*., The R882H DNMT3A mutation associated with AML dominantly inhibits wild-type DNMT3A by blocking its ability to form active tetramers. *Cancer Cell* **25**, 442–454 (2014).
47. I. Miller *et al*., Ki67 is a graded rather than a binary marker of proliferation versus quiescence. *Cell Rep.* **24**, 1105–1112.e5 (2018).
48. Y. Zou *et al*., Downregulation of DNA methyltransferase 3 alpha promotes cell proliferation and invasion of ectopic endometrial stromal cells in adenomyosis. *Gene* **604**, 41–47 (2017).
49. Q. Gao *et al*., Deletion of the de novo DNA methyltransferase Dnmt3a promotes lung tumor progression. *Proc. Natl. Acad. Sci. U.S.A.* **108**, 18061–18066 (2011).
50. S. F. Brunner *et al*., Somatic mutations and clonal dynamics in healthy and cirrhotic human liver. *Nature* **574**, 538–542 (2019).
51. I. Martincorena *et al*., Somatic mutant clones colonize the human esophagus with age. *Science* **362**, 911–917 (2018).
52. A. Yokoyama *et al*., Age-related remodelling of oesophageal epithelia by mutated cancer drivers. *Nature* **565**, 312–317 (2019).
53. K. Yoshida *et al*., Tobacco smoking and somatic mutations in human bronchial epithelium. *Nature* **578**, 266–272 (2020).
54. G. Genovese, S. Jaiswal, B. L. Ebert, S. A. McCarroll, Clonal hematopoiesis and blood-cancer risk. *N. Engl. J. Med.* **372**, 1071–1072 (2015).
55. C. J. Watson *et al*., The evolutionary dynamics and fitness landscape of clonal hematopoiesis. *Science* **367**, 1449–1454 (2020).
56. L. A. Miles *et al*., Single-cell mutation analysis of clonal evolution in myeloid malignancies. *Nature* **587**, 477–482 (2020).
57. K. Morita *et al*., Clonal evolution of acute myeloid leukemia revealed by high-throughput single-cell genomics. *Nat. Commun.* **11**, 5327 (2020).
58. S. Smemo *et al*., Obesity-associated variants within FTO form long-range functional connections with IRX3. *Nature* **507**, 371–375 (2014).
59. K. J. Sweeney *et al*., The first case report of medulloblastoma associated with Tatton-Brown-Rahman syndrome. *Am. J. Med. Genet. A.* **179**, 1357–1361 (2019).